RSC Advances

PAPER

View Article Online
View Journal | View Issue



Cite this: *RSC Adv.*, 2019, **9**, 924

# Photo-patterned oxygen sensing films based on Pt porphyrin for controlling cell growth and studying metabolism†

Fei Zeng,‡[a] Zengju Fan,‡[a] Shanshan Wu,*[b] Xing Cheng*[a] and Yanqing Tian *[a]

A new type of biocompatible and photo-polymerizable hydrogel with oxygen sensors for microengineering was developed. Herein, a red emitter as an oxygen probe which was chemically immobilized in a poly(2-hydroxyethyl methacrylate)-*co*-polyacrylamide-based matrix was expected to monitor cell metabolism. A few micropatterned films with gratings (5, 7, 10, 20, and 50 μm in width, respectively and with 1.2 μm in height) were designed and fabricated by photo-lithography using these hydrogels. SEM and AFM were used to validate these films to attain their lateral width and vertical depth. The oxygen responses of these films were characterized. Results showed that patterned films exhibited higher sensitivity than the non-patterned films. The films' construction can also have some influence on cell alignment and elongation. This phenomenon was evaluated by culturing human cervical cancer cells (HeLa cells) and mouse embryo fibroblasts (3T3-L1), on the film surfaces with different construction. Linear correlation between cell elongation and the logarithm of grating width was observed. Real-time monitoring of oxygen consumption of HeLa cells in cell culture medium was achieved. This study is expected to have potential to be applied in micro-structured design and to help understanding metabolism.

Received 8th November 2018
Accepted 23rd December 2018

DOI: 10.1039/c8ra09234f

rsc.li/rsc-advances



## 1. Introduction

In the micro-architecture of many tissues, dictating their biological and mechanical functions, surface properties which can control cellular alignment and elongation play a significant role. Some previous research demonstrated that the molecular, structural and electrophysiological properties of cardiac muscle would be affected by the complex organization of cardiomyocytes and fibroblasts within the cardiac extracellular matrix.[1] The circulatory system was shown to be influenced by the arrangement of differentiated myocytes within the musculoskeletal extracellular matrix.[2] Therefore, a system which can construct different functional extracellular matrices *in vitro* is highly required for effectively studying and imitating biological functions of many tissues.

Extracellular matrix (ECM) is deemed to affect the shape and direction of a large amount of mammalian cell types *in vitro*.[3–6] It is well known that surface forms the interface directly with the tissue, as a result, the surface properties, including topography and chemistry, are really of prime importance in resulting in the responses of cells and tissues to many kinds of biomaterials.[7] For instance, some researches have revealed that surface patterning have effects on cell elongation by designing different depths and widths of grooves on synthetic surfaces.[8] In addition, Clark *et al.* have illustrated that cell alignment seems to be a fairly more random reaction, especially on shallow grooves.[9] However, the inability to control cell behaviour precisely made it hard to construct a system using synthetic functional extracellular matrices to study cell behaviour and tissue function. Microscale technologies appear as powerful tools for controlling the cellular behaviour, including cell shape, growth and interactions by using surface patterning.[10] By controlling microenvironment, micro-topography together with synthetic extracellular matrix could tune the cell growth conditions more precisely. Better modulating on cell elongation, orientation, migration,[8] cell differentiation[11] and cell–cell interactions[12] are achieved with corresponding specific methods. Micro-engineering the surface of biologically relevant hydrogels has generated many new applications and implications in tissue engineering such as tissue architecture, vasoformation and cell seeding.[13]

On the other hand, hypoxia caused by low oxygen concentration is frequently observed in tumour tissues and proved to influence immunosuppressive pathways and may weaken tumour resistance.[14] This phenomenon is mainly ascribed to high consumption of cancer cells when they use energy.[15] A significant amount of previous work devoted to set up strategies

[a]*Department of Materials Science and Engineering, Southern University of Science and Technology, No. 1088 Xueyuan Blvd, Xili, Nanshan District, Shenzhen, Guangdong, 518055, China. E-mail: chengx@sustc.edu.cn; tianyq@sustc.edu.cn*

[b]*Guangdong Industry Polytechnic, No. 152 Xingang West Road, Haizhu District, Guangzhou, 510300, China. E-mail: 2018090123@gdip.edu.cn*

† Electronic supplementary information (ESI) available. See DOI: 10.1039/c8ra09234f

‡ Equal contribution.

for monitoring microenvironmental oxygen concentrations in physiological processes of living organisms.[16–18] Moreover, monitoring oxygen concentration in the surrounding environment is profitable in various fields like food production, fermentation industry and disease diagnosis.[19] Phosphorescent oxygen sensors have been widely used to monitor oxygen concentrations in real time.[20–23] However, until now, there is no report focusing on the development of micro-patterned oxygen sensing films as a novel type of ECM for cell alignment controlling and *in situ* real time monitoring cell respiration and even metabolism. We expect this new study will endow further insights on the understanding of cell metabolism using oxygen sensing films and generate new functional ECM.[24–27]

In this study, we have developed a new type of biocompatible and photo-polymerizable hydrogels with oxygen sensors for microengineering to achieve cell alignment controlling and cell respiration monitoring simultaneously. We used a modified platinum(II)-5,10,15,20-tetrakis-(2,3,4,5,6-pentafluorophenyl)-porphyrin (PtTFPP) possessing four methacrylate moieties (Fig. 1) as the oxygen probe, which is highly stable with efficient sensitivity.[24,28] In this kind of porphyrin, the Pt is suitable to increase the inter-system crosslinking,[28] and the fluorine substituents are to make it more stable as well as to increase its quantum efficiency.[24] This probe was polymerized into poly-acrylamide-*co*-poly(2-hydroxyethyl methacrylate) (PAM-*co*-PHEMA) matrices for preparing polymer-based oxygen sensing films with submicrometer topographic surface for achieving sensing and cell alignment controlling (Fig. 1). The sensing films were patterned using advanced photolithography and were designed to have gratings with different lateral width in micro-scale to stimulate and monitor cells (human cervical cancer HeLa cells and mouse embryo fibroblasts 3T3-L1 were used in this study) for understanding the influences of surface morphology on cell growth. It is expected that these new types advanced functional materials have potentials for controlling cell migration and cell proliferation as well as further altering cell metabolism.

## 2. Experimental

### 2.1 Materials and reagents

All chemicals and solvents listed below were analytically pure and were used without further purification. Trimethylolpropane ethoxylate triacrylate (SR454) and triethoxy-2-propenyl-silane (TMSPA) were obtained commercially from Sigma-Aldrich (Guangzhou, China). Phenylbis(2,4,6-trimethylbenzoyl) phosphine oxide (Photoinitiator-IrgCure 819) was purchased from Ryoji Organic Chemical (Shanghai, China). *N*′-*N*′-Dimethylformamide (DMF) and poly(ethylene glycol)dimethacrylate (PEGDMA, $M_n = 550$) were purchased from Xilong Scientific Inc. (Guangdong, China). Dimethyl sulfoxide (DMSO) was obtained commercially from DAMAO Chemical (Tianjin, China). 2-Hydroxyethyl methacrylate (HEMA) and acrylamide (AM) were purchased from LINGFENG Chemical reagents (Shanghai, China). Glucose was purchased from FUCHEN Chemical Reagents (Tianjin, China). Glucose Oxidase was acquired commercially from Aladdin (Shanghai, China). Photolithography printed photomasks was obtained commercially from the Institute of China electronics technology group CO., Ltd. Oxygen probe (OS, Fig. 1) was prepared according to known procedures.[24] Quartz glasses from University Wafer (South Boston, MA) were cut into squares of 13 mm × 13 mm using an advanced dicing system (ADS-800 Series, Optium).

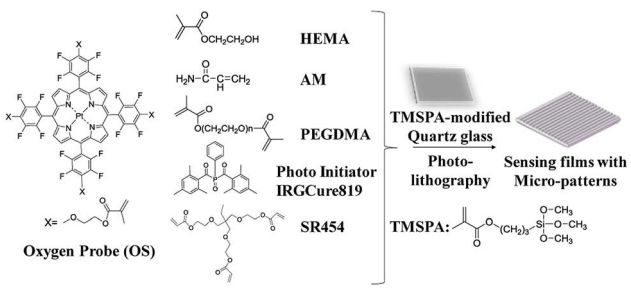


Fig. 1 Chemical structures of the oxygen probe (OS) and other monomers used for fabricating films and a simple scheme showing the process of micropatterned film fabrication.

### 2.2 Instruments

A LED-driving UV Curing System (Lamplic, Shenzhen, China) was used in curing process of photolithography. An oxygen plasma cleaner (Harrick Plasma, Ithaca, NY) was used for quartz glass surface activation. A Fluoromax-4 spectrofluorophotometer (Horiba Scientific Instruments) was used for phosphorescence measurements. A mask aligner (MA6BA6) was obtained from Germany. An ADS-800 Series advanced dicing system (Optium, Veeco, NY) was used for cutting quartz glass into squares of 13 mm × 13 mm, which can fit diagonally into a quartz fluorescence cuvette at an angle of 45° to the excitation light. A scanning electron microscopy (SEM, S-3000N, Hitachi) was utilized for characterization of film surface topography. An atomic force microscopy (AFM, Bruker Multimode 8) using Si-cantilevers with a resonance frequency in 70 kHz and a force constant in 0.4 N $m^{-1}$ (ScanAsyst mode, ambient atmosphere, room temperature) was utilized for analysis of surface roughness and topography. A laboratory water purification system (Master series, HITECH) was used to produce double distilled water. All experiments were accomplished at room temperature and 45–70% relative humidity except cell culture.

### 2.3 Fabrication of oxygen sensing films

The oxygen sensor films were prepared by several steps including the preparation of quartz glass, stock solution and fabrication of film structure *via* lithography (Fig. 1). The processes of preparation were based on our published protocol.[24] Detailed description of the preparation procedure of the micro-patterned films using photolithography was given in ESI (Fig. S1†).

HEMA (800 mg), SR454 (500 mg), AM (150 mg), PEGDMA (25 mg), photo-initiator (IrgCure-819) (10 mg) and OS (1 mg) were dissolved in DMF (0.5 mL) for preparing the stock solution for micro-patterned film fabrication. Stock solution (5 μL) was added onto a piece of (3-(trimethoxysilyl)propyl acrylate)

(TMSPA) modified quartz glass substrate. HEMA and AM are hydrogel precursors for forming hydrogel thin films after fabrication. SR454 and PEGDMA were used as crosslinkers to achieve highly mechanically stable films and could be polymerized induced by photo-initiator IrgCure-819 when stimulated by ultraviolet. The polymerization time was optimized to be 15 seconds. Because all the monomers including the OS were polymerized to form the films,[29] the oxygen probe has no leaching from the matrix.[24] After demolding and development in the acetone, photo-cured hydrogel patterned films with vertical depth of 1 μm and representative lateral width of 5 μm, 7 μm, 10 μm, 20 μm and 50 μm were obtained (Fig. S1c†). The lateral width was controlled as these values to fit diameters of most cell lines.[30] Thus, these films were suitable to investigate influence on various kinds of cells by these thin films. Oxygen probes were assembled onto surfaces of thin films.[31] After cut into unit piece by dicing-system, the final pattern layer on the silica wafer acted as our further research samples. The final films were dried and stored in the dark at room temperature ($23 \pm 2$ °C).

### 2.4 Sensor characterization

Sensing films with 13 mm × 13 mm dimensions were placed diagonally into a quartz cuvette with 2 mL of liquid (either a buffer or a medium) at an angle of 45° to the excitation light for emission measurement under a spectrofluorophotometer. A gas manifold for controlling gas flow was connected with the cuvettes to vary the concentrations of oxygen in the gaseous environment for oxygen titration and response time tests. The films were excited at 405 nm and the emission peaks at 645 nm were collected which were used for data analysis. For ensuring the components of gaseous environment stable when the film was tested under a certain oxygen concentration, the test won't be started until 3 minutes after changing the oxygen concentration.

### 2.5 Culture of cells for controlling alignment and elongation

Patterned films were sterilized by ultraviolet light at least 30 min and immersed in 75% alcohol at least 10 min before being taken into a biosafety cabinet. Phosphate-buffered saline (PBS; CORNING) was used to wash films for 10 times per piece. A cleaned film was put into a cell culture dish flatly with the quartz substrates adown. HeLa cells (purchased from GuangZhou Jennio Biotech Co., Ltd) and 3T3-L1 Fibroblasts (purchased from ATCC® CL-173™; it is a kind of fibroblast (biosafety level: 1) from embryo tissue of *Mus musculus* (mouse). It is a adherent cell line and was bought in frozen format.) cultured in Dulbecco's Modified Eagles Medium (DMEM; CORNING) supplemented with 10% fetal bovine serum (FBS; Gibco) and 1% penicillin–streptomycin solution (Gibco) were used as cell lines in this study for analysing influences on cell alignment and elongation by different film patterns. The cell concentration per film was around $10^4$ cells per mL. Cell line was incubated at 37 °C in 5% $CO_2$ humidified air balanced atmosphere. To assess the diameters of cells, over 10 individual cells were measured by NIH Image J software (NIH, Bethesda, MD) using microscopic images from at least 5 different sections of each film sample. At least 30 repeated experiments were conducted for each grating size.

### 2.6 Staining of HeLa cells for biocompatibility test

In order to test the biocompatibility of the micropatterned sensing films, Live/Dead Viability/Cytotoxicity Kit (L-3224) assay (for mammalian cell, Invitrogen Corporation) was utilized to stain HeLa cell grown on the films. Calcein AM (4 mM in anhydrous DMSO) and ethidium homodimer-1 (2 mM in DMSO/$H_2O$ solution) was diluted in cell culture medium to get the final concentration of 1 μM and 4 μM respectively.[25] Before staining, cells were cultured over 24 hours and washed with phosphate-buffered saline (PBS; CORNING) twice. After adding stains mentioned above, the cell culture dish was placed into incubator for 30 min until being imaged.

### 2.7 The use of sensors for *in situ* monitoring oxygen consumption by HeLa cells through metabolism process

The film with grating size of 20 μm in width was placed into a quartz cuvette like that in sensor characterization process with HeLa cell solution (2 mL) with concentration of $2 \times 10^6$, $1 \times 10^6$, and $2.5 \times 10^5$ (in cell culture medium), respectively. In order to separate air from medium, mineral oil (0.5 mL) was added on the top of medium in the cuvette. The measurements of emission intensities were taken per 0.01 second at 645 nm for about 25 min and films were excited at 405 nm.

## 3. Results and discussion

### 3.1 Film structural design and characterization

To evaluate the influences of grating physical properties, including the lateral width and vertical height, on phosphorescence sensing functions and cell growth conditions on films, patterned photo-cured hydrogel films with vertical depth of 1.2 μm and representative lateral width of 5 μm, 7 μm, 10 μm, 20 μm and 50 μm were prepared, respectively. Since lateral width of gratings may have different influence on various kinds of cells, the width of gratings ranging from 5 μm to 50 μm was designed to fit diameters of most cell lines.[30] Considering that our stock solution could not be fabricated into thin films by spin coating, spacers with 1 μm height was introduced on quartz glass *via* ICP etching to control film thicknesses. For controlling the cell growth, two parameters including the height and width of the patterning need to be considered. If vertical height of gratings was too miniscule, the distribution of cells on the sensing film would be random, which would make the influences of lateral width hard to observe. However, the fabrication of patterning with rather high gratings is time-consuming. Also, as some previous researches showed gratings with 1.2 μm in height are reasonable for cell growth controlling, we set this value in our design of film topography.[9]

SEM was used to characterize the patterned films (Fig. 2). A large area of gratings was observed with 5 μm-line/5 μm-space (or 7 μm, 10 μm, 20 μm and 50 μm) (Fig. 2a–e). Averaging results of testing values in repeated measurements have errors

 

within ±5% compared with their corresponding designed values. Therefore, results showed that the fabrication process of these thin films was reliable. However, since the main matrix of this kind of materials is hydrogel, which has low mechanical strength as reported in many previous studies,[32] these thin films would have significant deformation when applying force to cut films for getting a cross section of gratings. As a result, the height of gratings measured by SEM from the cross section (10 μm) might have a huge difference from its real depth (1 μm as designed) (Fig. 2f).

For further evaluating the micro-structures, atomic force microscopy (AFM) was used for analysis of vertical height of each kind of surface gratings. Due to the fact that thin films with grating width in 50 μm were too large to see a whole hollow and bulge *via* AFM, the heights of these films with 50 μm grating were not characterized by using AFM. Since all the films were designed to have the same heights and same fabrication processes, the real height of the films with grating width in 50 μm would be theoretically near to that of other kinds of films (Fig. S2†). In AFM results of films with width in 5 μm, 7 μm and 10 μm (Fig. S2a–S2c†), the edges of the gratings do not have a perpendicular profile like what can be observed in diagrams of films with width in 20 μm (Fig. S2d†). This phenomenon may be attributed to the larger surface tension existed in films with smaller grating width. Since they have larger contact area comparing with others, photo mask removal in the last fabrication process may be the cause of these defects. Despite all these detailed morphological structural differences, according to AFM images, height in these fabricated films was within a range of 1.2 μm ± 0.2 μm.

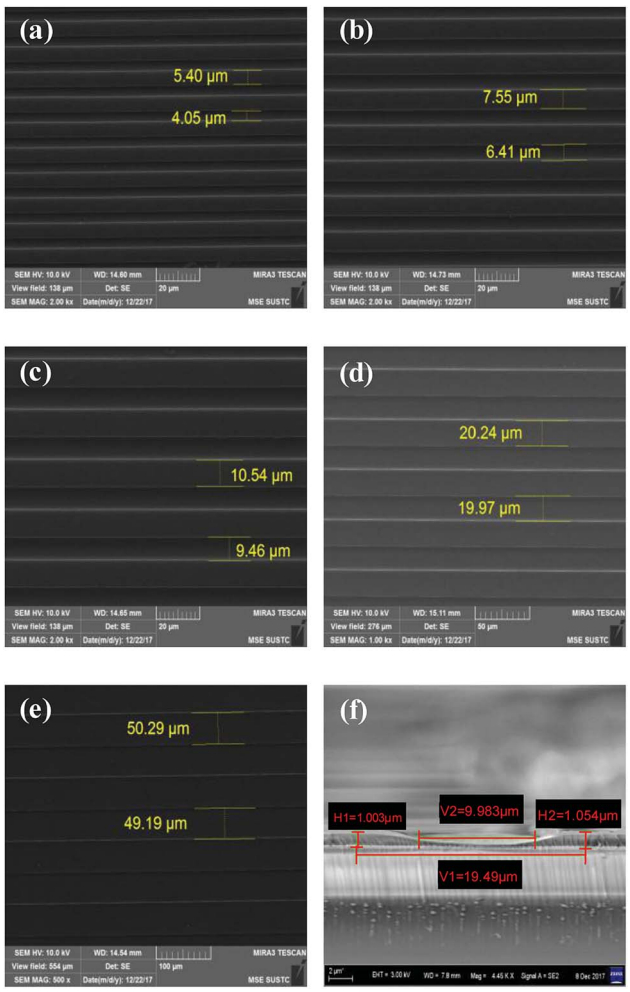


Fig. 2 SEM images of patterned films with grating width in 5 μm (a); 7 μm (b); 10 μm (c); 20 μm (d) and 50 μm (e). (f) SEM figure of cross-section of gratings with 10 μm in width and 1 μm in vertical height.

### 3.2 Sensing properties

Fig. 3a showed representative oxygen responses of a film with 10 μm width. Clear oxygen concentration-dependent emission intensity changes were observed. This was attributed to the distinctly increased quenching effect of the oxygen probes in films with oxygen. The sensors' responses followed Stern–Volmer equation (eqn (1)) (Fig. 3b).

$$\frac{I_0}{I} = 1 + K_{SV}[O_2] \quad (1)$$

where $K_{SV}$ is the Stern–Volmer quenching constant, $[O_2]$ is the dissolved oxygen concentration adjusted through the nitrogen and oxygen gas mixer. $I_0$ and $I$ are the emission intensities at 650 nm in deoxygenated condition and in certain oxygenated conditions, respectively.

It is obvious that the sensitivity of patterned films was much greater than that of unpatterned films, though there is no overt distinction among films with different grating width (Table 1). The better performances of these sensing films with micro-patterns could be attributed to their topographic surface, which ensures the oxygen sensors on the surface of hydrogel could efficiently interact with the DO *via* significantly enhancing specific surface area.[33] For oxygen sensing, oxygen permeability affects sensitivity – higher oxygen permeability will result in higher oxygen sensitivity. The patterned films possess more surface areas than the non-patterned films, this might to endow high oxygen permeability of the patterned films.

Response times of the films were also compared. Oxygen response time ($t_{95}$) is time interval for 95% of the total change in phosphorescence intensity from deoxygenated situation to 100% oxygenated situation. The recovery time ($t_{95\text{-r}}$) is time interval for 95% of the total change in phosphorescence

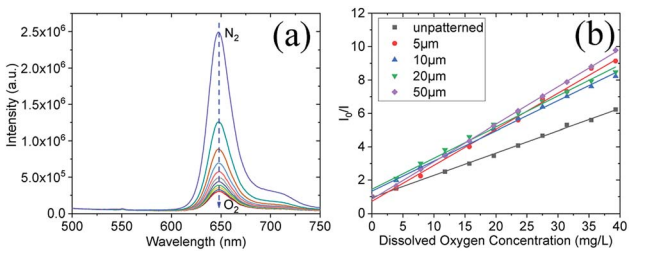


Fig. 3 Oxygen responses emission spectra of the film with 10 μm grating (a); Stern–Volmer plots for different sensing films with/without patterns at 25 °C (b).

Table 1 Comparison of response time and recovery time of films with different grating widths

| Films | Response time ($t_{95}$) | Recovery time ($t_{95\text{-r}}$) |
|---|---|---|
| Non-patterned | 183.1 s | 10.1 s |
| 5 μm grating | 134.8 s | 7.2 s |
| 10 μm grating | 96.6 s | 10.2 s |
| 20 μm grating | 84.5 s | 7.2 s |
| 50 μm grating | 68.4 s | 9.9 s |

intensity switching from oxygenated situation to deoxygenated situation. Results showed that response times to oxygen ($t_{95}$) are quite similar in the same range from 7.2 s to 10.2 s. The recovery time ($t_{95\text{-r}}$) of each patterned film is faster than the of non-patterned film, however there is no clear tend to show the pattern grating width's influence on the recovery time (Fig. S3† and Table 1).

### 3.3 Cells growth on the films

To investigate the influence of grating width on cell alignment and elongation, HeLa cells and 3T3-L1 fibroblasts as representative mammalian cells were used and cultured on these micro-patterned thin films. All of the films with cells were observed under a phase contrast fluorescent inverted microscope since the thickness of quartz glass is out of focus range of high resolution microscope such as laser confocal fluorescence microscope. Cells proliferated well on the film surface; however, grating width affected cell alignment and elongation.

For HeLa cells, the situation cells randomly attached on unpatterned film looked like that of cells grown on the bottom of normal cell culture dish (Fig. 4a). It was observed that "antennaes" of cells attached on gratings alternatively, which means that most of cells attached on hollows or most of them grew on bulges of the patterned films (Fig. 4b and c). Since widths of hollows and bulges are almost the same, it is impossible to determine where most cells attached *via* these optical microscopic images. To explore this question, bright field microscopic image of the oxygen sensing film with grating width in 50 μm (Fig. S4a†) was overlapped on its phosphorescent images in the same view (Fig. S4b†). By referring the red emission from the sensors excited at 405 nm (Fig. S4c†), the result illustrated that most of "antennaes" of cells attached on bulges of films. In other words, most of the cells seeded attached on the top surfaces of our biocompatible sensing materials.

Most of Hela cells elongated longer and tended to align parallel to gratings (Fig. 4b and c). To gain a more precise relationship between grating width as well as cell elongation and alignment for cells, 30 repeated experiments were conducted for each grating size. Then, NIH ImageJ software was utilized to analyze elongation and alignment situation of every whole cell with clear edge in images. In this analytical process, elongation situation of HeLa cells was characterized by length of cell long axis ($a$, Fig. S5†) over length of cell short axis ($b$, Fig. S5†) and alignment of cell was judged by included angel between direction of cell long axis and grating on film ($\alpha$, Fig. S5†). From comparison of the average

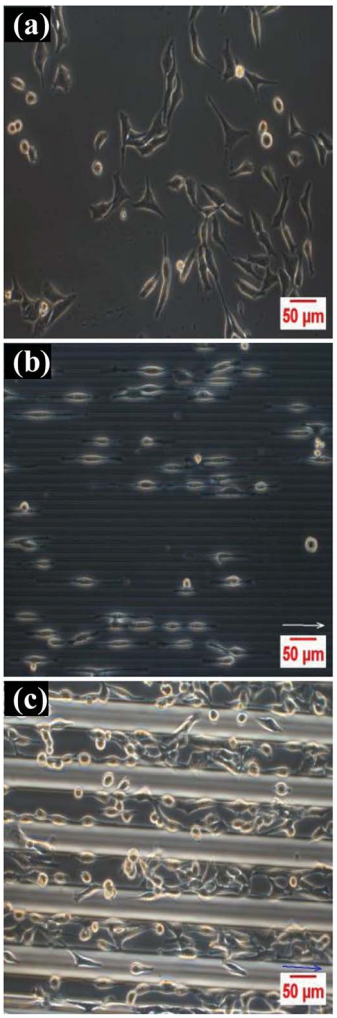


Fig. 4 Cell attachments after 24 hours culture on the non-patterned film (a), 5 μm featured patterned film (b), and 50 μm featured patterned film (c) for HeLa cells.

elongation ratios ($a$/$b$, Fig. S5†) of results for each group, we found that elongation ratios ($a$/$b$, Fig. S5†) of HeLa cells grown on these sensing films decreased with increasing of grating width (Fig. 5a). When the elongation ratios for cells on films were linear fitted with logarithm of their corresponding grating width, the result showed that they had high linear relevance (Fig. 5b). This relevance may can help us design new structures of films to guide cell growth or even cell differentiation.

The alignments of HeLa cells grown on these micro-patterned sensing films demonstrated that cells tended to align along grating directions on films with smaller grating width. The average angle ($\alpha$, Fig. S5†) between the direction of cells' long axis and the direction of grating on films is smaller than 3 degrees for the films with grating width smaller than or equal to 10 μm, which shows their excellent ability in guiding the cell alignment (Fig. 5c). It was reported that different elongation conditions of cells would guide stem cells differentiation into different cells in some studies.[34,35] Thus the novel materials reported herein may be developed to control cell differentiation.

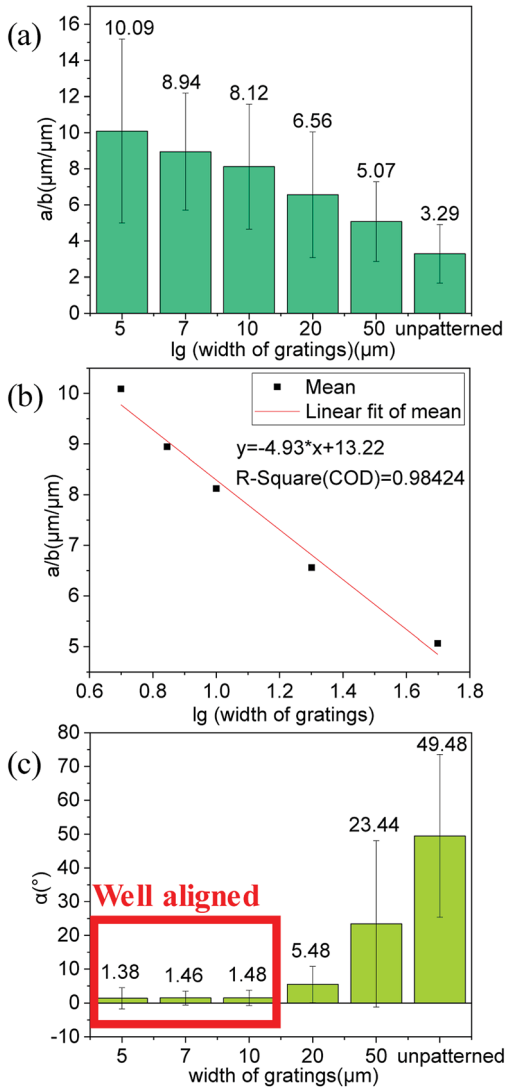


Fig. 5 (a) Average elongation ratios (*a*/*b*, Fig. S5†) and corresponding standard deviations for cells on various films. (b) Linear fitted plot of elongation ratios (*a*/*b*, Fig. S5†) for cells on films with logarithm of their corresponding grating widths. (c) Average included angle ($\alpha$, Fig. S5†) and corresponding standard deviations between direction of cell long axis and grating on films for cells.

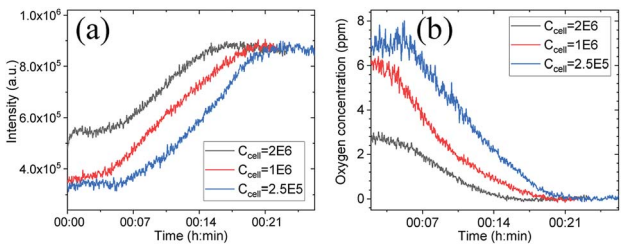


Fig. 6 Emission changes of the sensing film in culture medium with suspended HeLa (a) and corresponding calculated oxygen concentration changes (b).

Another cell line was also tested by using 3T3-L1 fibroblasts. However, for 3T3-L1 fibroblasts, 3T3-L1 fibroblasts formed extensive "cell-strips" along the 50 μm grating (Fig. S6b†), and big "cell-sheets" upon the 5 μm grating surface (Fig. S6c†). 3T3-L1 fibroblasts tends to get together when grating width of film becomes smaller. This phenomenon may attribute to stronger connection between fibroblasts compared to that of HeLa, which is a kind of epithelial cell.[36] As a result, 3T3-L1 fibroblasts preferred attaching to each other to form cell-strips or -sheets. This makes it possible for us to design thin film 3D multi-layer structure using this material for inducing 3T3-L1 fibroblasts grow into tissue *in vitro*.[37–39]

### 3.4 Biocompatibility test

Cell viability kit was utilized to discern any potential cytotoxicity influenced by the lithography patterned sensing films. Calcein AM in the Live/Dead cell kit is cell permeable and its de-ester derivative exhibits green emission for only live cells. The other dye EthD-1, which only enters dead cells with damaged membranes, thereby producing a bright red fluorescence in dead cell.[25] Almost only green emission from cells was observed, showing the minimum-cytotoxicity of the sensing films. (Fig. S7†). Through the counting of the cell ratios with green and red emission, almost 100% live cells were quantitatively observed, further demonstrating the high biocompatibility of the sensing films.

### 3.5 *In situ* monitoring oxygen consumption by HeLa cell

For further demonstrating the capability of patterned sensing films for monitoring dissolved oxygen, a representative film with 20 μm grating width was put in a quartz cuvette filled with HeLa cells at different concentrations. For shortening the experimental time, a layer of mineral oil was added on the top of the medium. Real-time emission intensity change by cells was given in Fig. 6a. It was observed that more cells can consume oxygen faster. By referring the titration Stern–Volmer curve, oxygen concentration was calculated and illustrated in Fig. 6b. The results indicated the potential application of the micro-patterned sensing films for real-time monitoring oxygen consumption for metabolism understanding.

## 4. Conclusions

A novel type of biocompatible and photo-polymerizable hydrogels with oxygen sensors was developed in this study. The hydrogel-based sensors were successfully fabricated to different lateral widths by photolithography. Sensors' sensitivity and response time were evaluated. Sensing films with grating patterns were proved to have higher sensitivity for oxygen than that of the unpatterned film. Live and Dead kit was used to testify that films are nontoxic to HeLa cells so that this kind of hydrogel is biocompatible. Hela cells and 3T3-L1 as representative cells were cultured on these sensing films. Results revealed that grating widths affected or controlled certain kinds of cell alignment and elongation. Inspiration from these results illuminates us to further investigate suitable grating width to control artificial tissue forming and stem cells directed differentiation. These sensing films were demonstrated to have the capability for monitoring oxygen consumption in real-time by

mammalian cells. Further work is in progress to culture stem cells on films with various topographic surfaces to induce differentiation, while monitor the metabolism changes of them in the meantime.

## Conflicts of interest

There are no conflicts to declare.

## Acknowledgements

Authors would like to thank the supports from National Natural Science Foundation of China (21604036, 21574061), Shenzhen fundamental research programs (JCYJ20170412152922553), the High-level university construction fund for SUSTech (G01256018), and Shenzhen fundamental research programs (JCYJ20160301114303878).

## References

1 M. Papadaki, N. Bursac, R. Langer, J. Merok, G. Vunjak-Novakovic and L. E. Freed, *Am. J. Physiol.: Heart Circ. Physiol.*, 2001, **280**, H168–H178.
2 J. J. Chiu, L. J. Chen, C. N. Chen, P. L. Lee and C. I. Lee, *J. Biomech.*, 2004, **37**, 531–539.
3 B. Weyand, K. Reimers and P. M. Vogt, *Presented in part at the 8th Int. Conf. Cell & Stem Cell Eng. (ICCE)*, 2011.
4 K. Bhadriraju and L. K. Hansen, *Exp. Cell Res.*, 2002, **278**, 92–100.
5 M. Pulina, D. Liang and S. Astrof, *Biol. Open*, 2014, **3**, 583–590.
6 R. K. Schneider, J. Anraths, R. Kramann, J. Bornemann, M. Bovi, R. Knüchel and S. Neuss, *Biomaterials*, 2010, **31**, 7948–7959.
7 D. M. Brunette and B. Chehroudi, *J. Biomech. Eng.*, 1999, **121**, 49–57.
8 K. Lee, E. H. Kim, N. Oh, N. A. Tuan, N. H. Bae, S. J. Lee, K. G. Lee, C.-Y. Eom, E. K. Yim and S. Park, *J. Nanobiotechnol.*, 2016, **14**, 35.
9 P. Clark, P. Connolly, A. S. Curtis, J. A. Dow and C. D. Wilkinson, *Development*, 1990, **108**, 635–644.
10 A. Khademhosseini, R. Langer, J. Borenstein and J. P. Vacanti, *Proc. Natl. Acad. Sci. U. S. A.*, 2006, **103**, 2480–2487.
11 J. A. Burdick and G. Vunjak-Novakovic, *Tissue Eng., Part A*, 2009, **15**, 205–219.
12 Y. Ito, M. Hayashi and Y. Imanishi, *J. Biomater. Sci., Polym. Ed.*, 2001, **12**, 367–378.
13 A. Khademhosseini and R. Langer, *Biomaterials*, 2007, **28**, 5087–5092.
14 M. Z. Noman, M. Hasmim, Y. Messai, S. Terry, C. Kieda, B. Janji and S. Chouaib, *Am. J. Physiol.: Heart Circ. Physiol.*, 2015, **309**, C569–C579.
15 J. L. Thorne and M. J. Campbell, *Int. J. Cancer*, 2015, **137**, 1519–1527.
16 V. S. Whiffin, M. J. Cooney and R. Cord-Ruwisch, *Biotechnol. Bioeng.*, 2004, **85**, 422–433.
17 A. Nygren, K. Rennerfelt and Q. Zhang, *J. Clin. Monit. Comput.*, 2014, **28**, 57–62.
18 J. A. Scaringi, A. O. Rosa, M. Morad and L. Cleemann, *J. Appl. Physiol.*, 2013, **115**, 1855–1861.
19 K. Zhang, H. Zhang, W. Li, Y. Tian, S. Li, J. Zhao and Y. Li, *Mater. Lett.*, 2016, **172**, 112–115.
20 T. Yoshihara, Y. Yamaguchi, M. Hosaka, T. Takeuchi and S. Tobita, *Angew. Chem.*, 2012, **124**, 4224–4227.
21 T. C. O'Riordan, D. Buckley, V. Ogurtsov, R. O'Connor and D. B. Papkovsky, *Anal. Biochem.*, 2000, **278**, 221–227.
22 J. Alderman, J. Hynes, S. M. Floyd, J. Kruger, R. O'Connor and D. B. Papkovsky, *Biosens. Bioelectron.*, 2004, **19**, 1529–1535.
23 S. Banerjee, C. Kelly, J. P. Kerry and D. B. Papkovsky, *Trends Food Sci. Technol.*, 2016, **50**, 85–102.
24 Y. Tian, B. R. Shumway and D. R. Meldrum, *Chem. Mater.*, 2010, **22**, 2069–2078.
25 P. C. Thomas, M. Halter, A. Tona, S. R. Raghavan, A. L. Plant and S. P. Forry, *Anal. Chem.*, 2009, **81**, 9239–9246.
26 A. Weltin, K. Slotwinski, J. Kieninger, I. Moser, G. Jobst, M. Wego, R. Ehret and G. A. Urban, *Lab Chip*, 2014, **14**, 138–146.
27 Y. Tian, B. R. Shumway, W. Gao, C. Youngbull, M. R. Holl, R. H. Johnson and D. R. Meldrum, *Sens. Actuators, B*, 2010, **150**, 579–587.
28 E. Onal, Z. Ay, Z. Yel, K. Ertekin, A. G. Gurek, S. Z. Topal and C. Hirel, *RSC Adv.*, 2016, **6**, 9967–9977.
29 Y. Qian, B. Liu, W. Duan and Q. Zeng, *J. Porphyrins Phthalocyanines*, 2018, **22**, 717–725.
30 S. N. Lawson, K. W. T. Caddy and T. J. Biscoe, *Cell Tissue Res.*, 1974, **153**, 399–413.
31 Y. T. Shen, K. Deng, X. M. Zhang, D. Lei, Y. Xia, Q. D. Zeng and C. Wang, *J. Phys. Chem. C*, 2011, **115**, 19696–19701.
32 J. M. Seidel and S. M. Malmonge, *Mater. Res.*, 2000, **3**, 79–83.
33 Y. Y. Mao, Q. Zhao, T. T. Pan, J. Y. Shi, S. M. Jiang, M. W. Chen, B. P. Zhou and Y. Q. Tian, *New J. Chem.*, 2017, **41**, 5429–5435.
34 Y. Shi, K. L. Zhou, W. J. Zhang, Z. Y. Zhang, G. D. Zhou, Y. L. Cao and W. Liu, *Biomed. Mater.*, 2017, **12**, 11.
35 Y. F. Rui, P. P. Y. Lui, Y. M. Wong, Q. Tan and K. M. Chan, *J. Orthop. Res.*, 2013, **31**, 746–753.
36 S. Yonemura, M. Itoh, A. Nagafuchi and S. Tsukita, *J. Cell Sci.*, 1995, **108**, 127–142.
37 L. H. Nguyen, A. K. Kudva, N. S. Saxena and K. Roy, *Biomaterials*, 2011, **32**, 6946–6952.
38 L. G. Griffith and M. A. Swartz, *Nat. Rev. Mol. Cell Biol.*, 2006, **7**, 211–224.
39 V. Chan, P. Zorlutuna, J. H. Jeong, H. Kong and R. Bashir, *Lab Chip*, 2010, **10**, 2062–2070.